HHS Public Access

Author manuscript

J Mol Biol. Author manuscript; available in PMC 2018 August 04.

Published in final edited form as:

J Mol Biol. 2017 August 04; 429(16): 2571–2589. doi:10.1016/j.jmb.2017.06.011.

Dynamic Modulation of Binding Affinity as a Mechanism for Regulating Interferon Signaling

Hongchun Li[1,*], **Nanaocha Sharma**[2,*], **Ignacio J. General**[1,3], **Gideon Schreiber**[2], and **Ivet Bahar**[1]

[1]Department of Computational and Systems Biology, School of Medicine, University of Pittsburgh

[2]Department of Biomolecular Sciences, Weizmann Institute of Science, Rehovot, Israel

[3]School of Science and Technology, and CONICET, Universidad Nacional de San Martin, San Martin, Buenos Aires, Argentina

Abstract

How structural dynamics affects cytokine signaling is under debate. Here, we investigated the dynamics of the type I interferon (IFN) receptor, IFNAR1, and its effect on signaling upon binding IFN and IFNAR2 using a combination of structure-based mechanistic studies, *in situ* binding and gene induction assays. Our study reveals that IFNAR1 flexibility modulates ligand-binding affinity, which, in turn, regulates biological signaling. We identified the hinge sites and key interactions implicated in IFNAR1 inter-subdomain (SD1-SD4) movements. We showed that the predicted cooperative movements are essential to accommodate intermolecular interactions. Engineered disulfide bridges, computationally predicted to interfere with IFNAR1 dynamics, were experimentally confirmed. Notably, introducing disulfide bonds between subdomains SD2 and SD3 modulated IFN binding and activity in accordance with the relative attenuation of cooperative movements with varying distance from the hinge center; whereas locking the SD3-SD4 interface flexibility in favor of an extended conformer increased activity.

Graphical abstract

Corresponding authors: gideon.schreiber@weizmann.ac.il, bahar@pitt.edu.
*co-first authors; contributed equally to the paper

Author contributions

GS and IB designed the study and wrote the first draft of the manuscript, NS did the experiments: HL and IJG did the computations. All authors analyzed the data, and contributed to editing and revising the manuscript, figures and animations.

Conflict of interest

The authors do not have a conflict of interest.

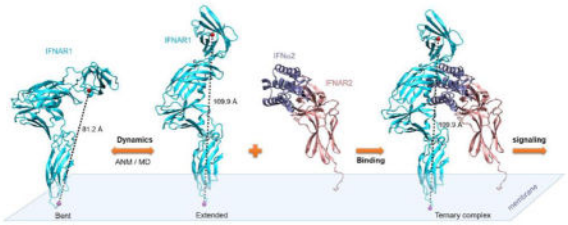

Keywords

conformational flexibility; elastic network models; interferon binding affinity; regulation of cytokine signaling; structural dynamics

Introduction

Type I interferons (IFNs) are members of the cytokine family mediating diverse biological and cellular responses such as resistance to viral infections, regulation of cell survival, promotion of antitumor activities, and immune response modulation (Platanias, 2005). IFNs induce a cellular response upon forming a ternary complex with two surface receptors, IFNAR1 and IFNAR2 (Thomas *et al.*, 2011). Binding of IFN to the extracellular (EC) domains of these receptors results in bringing their intracellular (IC) domains into close proximity, upon which their associated tyrosine kinases (JAKs) phosphorylate IC receptor chains and associated effector proteins (Stark and Darnell, 2012; Sharma *et al.*, 2016).

Recently we have shown that IFN activation does not require specific conformational changes transmitted from the outside to the inside of the cell, suggesting that JAK/STAT activation is a function of the ligand-driven proximity and the duration of engagement (Sharma *et al.*, 2016). The family of IFNs comprises sixteen members in humans (Uze *et al.*, 2007), which are not all functionally redundant (Brierley and Fish, 2002; Foster *et al.*, 2004; Severa *et al.*, 2006; Jaks *et al.*, 2007; Marijanovic *et al.*, 2007; Kalinke and Prinz, 2012). The main difference between the IFNs is in their binding affinity to each of the receptor chains, which ranges from nM to μM for IFNAR2 and from 0.05–10 μM for IFNAR1 (Lavoie *et al.*, 2011). The much lower affinity to IFNAR1 is conserved in all IFNs. IFNβ has overall a substantially higher affinity to the cell surface receptor, which has a decisive role for the pronounced differential cellular activities of IFNβ (Schreiber and Piehler, 2015). We have shown that engineering the binding affinity of IFNα2 to mimic the affinities of the different type I IFNs mimics their differential modes of activation (Jaitin *et al.*, 2006; Kalie *et al.*, 2007; Lavoie *et al.*, 2011; Thomas *et al.*, 2011; Schreiber and Piehler, 2015). In addition to binding affinity, the duration of receptor engagement and the concentration of the surface receptor are major determinants of differential activity. While weak and transient binding to few receptors is sufficient to induce robust activities (such as antiviral), tight and prolonged binding to a high percentage of IFN receptors is required to induce tunable (antiproliferative, immunomodulatory) activities (Levin *et al.*, 2011, 2014). Robust IFN activation is observed in all cell lines, while tunable activities are cell line specific. These activities are related to the induction of specific sets of genes (robust versus tunable genes) (Levin *et al.*, 2014).

IFNAR1 and IFNAR2 are both transmembrane (TM) proteins that belong to the class II helical cytokine receptors (Kotenko and Langer, 2004; Uze *et al.*, 2007). Their EC domains comprise four (SD1-SD4) and two (SD1-SD2) fibronectin type III-like subdomains, respectively (Novick *et al.*, 1994). The structures of two heterotrimeric complexes (containing IFNAR1 and IFNAR2) in the presence of IFNω, and a tight binding IFNα2 mutant (YNS) have been determined by X-ray crystallography. Despite the different physiological activities of the two ligands, the heterotrimeric complex shares the same architecture as all type I IFNs. In addition, high-resolution structures of unliganded IFNAR1 and IFNAR2, IFNα2-IFNAR2 and mouse IFNAR1-IFNβ complexes have been determined (Thomas *et al.*, 2011; de Weerd *et al.*, 2013). The latter is the only structure where the subdomain SD4 of IFNAR1 was resolved. Fig. 1 illustrates this architecture for the complex IFNAR1-IFNα2-IFNAR2, reconstructed using existing structural data (Thomas *et al.*, 2011), and the lipid bilayer and TM helices modeled *in silico*. The IFNAR1-IFN interface is formed by residues belonging to the IFNAR1 subdomains SD1, SD2, and SD3. SD4 is not directly involved, although it is computationally observed that SD4 enjoys an enhanced mobility and can get close to IFN and interact with it.

Comparison of unbound IFNAR1 with its IFN-bound form reveals a large rearrangement in the EC subdomains SD1-SD4 (Thomas *et al.*, 2011). Structural movements of receptor components upon ligand binding have previously been implicated in signal propagation across the membrane. In the case of IFNAR1, a conformational change was first observed by FRET (Strunk *et al.*, 2008b), which showed an increase of ~12 Å in the distance between the C - and N-terminal domains upon ligand binding, thus stabilizing a relatively ‘extended’ conformation of IFNAR1 subdomains, as opposed to a compact/closed conformation in the unbound state. Moreover, it was established that the ligand-induced conformational changes propagated to the membrane-proximal Ig domain of IFNAR1, which does not interact with the ligand. This was shown by an electron transfer-sensitive fluorescence dye attached covalently to residue N349C (Strunk *et al.*, 2008a, 2008b). Fluorescence quenching of this dye by a neighboring tryptophan (Trp347) was abrogated upon IFN binding, suggesting that the accessibility of this Trp was altered by a conformational change. Both global and local conformational changes were observed for IFNα2 and IFNβ. While the conformational changes at the EC region of IFNAR1 may be important, IFN signaling remains intact when the TM helix connecting the EC and IC IFNAR1 domains was mutated in any possible way (Sharma *et al.*, 2016), presumably due to the unstructured segments flanking the TM domain on both sides.

Our aim here is to elucidate the significance of the IFNAR1 receptor flexibility in IFN signaling. As shown by us previously, it is unlikely that the movements of the EC domain will affect the arrangement of the IC domain (Sharma *et al.*, 2016). However, such movements may be essential to mediating ligand specificity and binding affinity, and may affect signaling functions. We studied here the conformational dynamics of IFNAR1 and its ternary complex with the help of computational and experimental methods designed to probe the specific role of particular interactions in controlling biochemical (binding) and biological (signaling) responses. First, we characterized the structure-encoded dynamics of IFNAR1 and its ternary complex, and identified the hinge sites and key interactions that mediate inter-subdomain movements, using the Gaussian network model (GNM) and the anisotropic

network model (ANM) (Bahar *et al.*, 1997; Atilgan *et al.*, 2001; Eyal *et al.*, 2015; Li *et al.*, 2016), complemented by molecular dynamics (MD) simulations. Next, we examined the effect of hindering these movements by a set of disulfide bridges inserted at those key residue pairs, and we evaluated experimentally the consequence on IFN-binding affinity and the potential of IFNAR1 to transduce a signal. The results clearly show that restricting the EC interdomain movements affects binding affinity, which in turn, affect signaling. Thus, we present a new concept in signal transduction, where affinity is tuned by receptor flexibility, and this in turn modulates biological signaling.

Results

In silico identification of key mechanical sites that mediate interdomain movements in IFNAR1

We first provide a glimpse into the collective motions of IFNAR1 and its complex with IFN and IFNAR2, predicted by the ANM. Our analysis highlights the intrinsic ability of the IFNAR1 to undergo cooperative structural changes between compact and extended forms. Fig. 2 and Animations 1 and 2 illustrate the two most cooperative (global) modes of motions predicted for IFNAR1, referred to as modes 1 and 2. These modes define the most readily accessible, or softest, changes in structure uniquely favored by the native contact topology (see Methods).

Mode 1 (Fig. 2a; Animation 1) is a bending motion, where the subdomains SD1 and SD2 are rotated with respect to the subdomains SD3 and SD4 (attached to the membrane); the interfacial region between SD2 and SD3 harbors a hinge center that mediates the movements of the two halves of the molecule in this mode. A number of residue pairs that make inter-subdomain contacts are shown at the interface: E211-F290 (*blue*/*gray*), Y163-E293 (*magenta*), L134-R241 (*green*) and G133-F238 (*cyan*). Mode 2 (Fig. 2b; Animation 2), on the other hand, involves a hinge-bending region at the interface between SD3 and SD4, in addition to a moderate flexibility at the SD1-SD2 interface. Two glutamines, Q268 and Q328 (*green*), located near hinge site at the SD3-SD4 interface, will be shown below to play a key role in mediating inter-subdomain flexibility.

Both modes enable the receptor to undergo significant fluctuations (of about ± 14Å) in the distance between the subdomains SD1 and SD4, as shown in the figures and animations. These are comparable to the changes in the distance between N23 and T407 observed in FRET experiments (~12 Å) upon ligand binding (Strunk *et al.*, 2008a, 2008b). The modes intrinsically accessible to IFNAR1 unbound structure are therefore used by the receptor for IFN binding, similar to the observations made earlier for unbound and bound forms of enzymes (Tobi and Bahar, 2005).

ANM analysis repeated in the presence of IFNAR2, IFNα2, and the lipid bilayer showed that the intrinsic dynamics of IFNAR1 is largely retained in the heterotrimeric complex. The lipid bilayer was modeled using the *MembrANM* module of the *ProDy* application programming interface (Bakan *et al.*, 2011), as described in the Methods. Fig. S1 shows the correlation cosine between the modes accessible to IFNAR1 in isolated state and those in the presence of IFNAR2, IFNα2, and the lipid bilayer. As can be seen from the color-code (*right*

bar) mode-mode correlation map, the lowest frequency modes of IFNAR1 (*ordinate*) are retained with a correlation cosine of ≥ 0.75 in the ternary complex (*abscissa*).

IFNAR1 optimizes its interaction with interferon by exploiting its ability to reconfigure between extended and bent conformers

We have previously shown a substantial receptor rearrangement of IFNAR1 upon IFN binding. Here, we focus on the significance of the softest ANM modes in enabling the precise structural change observed in IFNAR1 upon IFN binding. As shown above, both modes 1 and 2 induce significant flexibility in IFNAR1. In addition, ANM mode 4 is found to facilitate the transition of IFNAR1 between its IFN-bound (PDB id: **3SE3**) and -unbound (PDB id: **3S98** with modeled SD4) forms. Fig. 3a depicts the superposition of the known unbound (*green*) and IFN-bound (IFNAR1 in *cyan*, and IFN in *blue/gray*) structures. The unbound and bound forms of IFNAR1 differ by an RMSD of 4.1 Å. Now, suppose we take the unbound form and deform it along ANM mode 4. The direction of deformation is shown by the *orange arrows* in Fig. 3b. The resulting conformation, shown in Fig. 3c (*orange*), exhibits an RMSD of 2.3 Å from the bound form. Therefore, ANM mode 4 facilitates the reconfiguration of (the unbound) IFNAR1 toward its conformer stabilized upon binding its substrate. Animation 3 illustrates the structural change along this mode.

We further verified the accessibility of the bent conformer of IFNAR1 starting from the extended conformer, as well the adaptability of the structure to optimize its binding with IFN, by examining the softest deformations predicted by the ANM in the presence of IFNAR2, IFNα2, and the lipid bilayer. The results presented in Fig. 4 and Animation 4 show the ability of the complex to undergo concerted movements between extended and compact forms of IFNAR1, while maintaining its close association with its substrate and associated receptor IFNAR2.

Restricting the movements SD4 relative to SD3 affects IFN binding

Both experimental and computational studies suggest SD4 to move relatively easily around its hinge region. Therefore, restricting the interdomain movements by introducing a disulfide bridge between them should be of consequence. As shown in Fig. 2b, Q268 (SD3) and Q328 (SD4) occupy the close vicinity of the SD3-SD4 hinge region, and their distance is altered during the global modes of motion. In the bound form, the mutation of these glutamines to cysteines is expected to form a disulfide bridge per the model of human IFNAR1 (Fig. 5a). To validate the formation of a disulfide bond between these two cysteines, we expressed and purified the mutant protein and subjected it to mass spectrometry after digestion of IFNAR1 with chymotrypsin as detailed in Materials and Methods. The resulting mass data were searched with MassMatrix using disulfide exploratory search parameters. Fig. 5b shows that the only two disulfide bonds clearly identified were between residues 268 and 328, and residues 172 and 193, the latter being a native disulfide of the receptor. Apparently, the other native disulfide bonds were not identified as the digestion was performed under native conditions, and only these two disulfide bonds are surface exposed. The disulfide bond was further validated by adding maleimide alexa flour 647 to IFNAR1, showing C268 and C328 to be oxidized (see Materials and Methods).

The movement of SD4 upon IFN binding was previously monitored through electron transfer from a fluorescence dye (ATTO655) attached covalently to N349C (Strunk *et al.*, 2008a, 2008b). Fluorescence quenching of this dye by the neighboring Trp347 is abrogated upon IFN binding, suggesting that the accessibility of this tryptophan is altered by a conformational change. After formation of the 268–328 disulfide bond, the fluorescence quenching of Trp347 did not change upon IFN binding (Fig. 5c), suggesting that the disulfide bond formed in this double mutant (referred to as SD34 mutant) locks the vicinity of these residues in a fixed conformer.

To investigate whether the conformation stabilized upon cross-linking C268 and C328 was closer to the bound or unbound structures of IFNAR1, we performed a series of molecular dynamics (MD) simulations, using the wild type and double-mutant IFNAR1, in isolation and in ternary complexes. The simulations clearly showed that an extended conformation was stabilized by the double mutant (shown in Fig. 5e), in contrast to the more compact form preferred by the wild-type receptor (Fig. 5d). The extended conformation is the preferred form of IFNAR1 in its IFN-bound state. The simulations were initiated from human IFNAR1- IFNα2- IFNAR2 complex (*white*, only IFNAR1 is shown) and repeated with the wild-type (WT) and double-mutant (SD34) IFNAR1. The distance between SD1 and SD4, represented by N23 (*red sphere*) and T407 (*magenta sphere*) reduces from 107.4 to 95.4 Å in the WT (consistent with FRET observations mentioned above); while the distance between the same pair of residues practically remains unchanged in SD34 (Fig. 5f).

The effect of the disulfide bond between SD3 and SD4 on IFN binding was further measured by surface plasmon resonance (SPR) with the purified receptor bound to the sensor chip. Fig. 6a and Fig. S2 1a and b and Table S1 show a 4-fold increase in binding affinity between the high affinity IFNα2-YNS mutant and IFNAR1 Q268C-Q328C with respect to the WT receptor. A similar increase in binding affinity is observed with IFNα2 as well (Fig. S2 1c and d).

Restricting the movements of SD4 relative to SD3 increases the efficacy of interferon signaling

Previous work has consistently shown a relation between binding affinity and biological activity, however, these were for mutants that directly affected IFN binding. Here, we determined the potency of the Q268C-Q328C double mutant to activate specific IFN induced activities on Huh7 cells, lacking endogenous IFNAR1 and with the mutant or wild-type receptors stably transfected (Sharma *et al.*, 2016). In line with its increased binding affinity (Fig. 6a), the EC50 for IFN inducing antiviral activity of Huh7 cells was ~7-fold lower for Q268C-Q328C in comparison to the wild-type receptor (Fig. 6b). Monitoring IFI6 and MX1 gene induction showed a ~4-fold lower EC50 for the mutant receptor than for wild-type (Fig. 6c). Using the Fluidigm system to evaluate the induction of a wider set of genes by IFN verifies the increased efficacy for the Q268C-Q328C double mutant (Fig. 6e).

To verify that the increased efficacy is a result of the disulfide bridge between C268 and C328, we measured the potency of the two single mutant IFNAR1 receptors to transmit a signal. As seen in Fig. 6D and E, the single mutants decreased gene induction, and thus reduced the signaling through the receptor. All the above data clearly demonstrates that

conformational restriction of IFNAR1 at the SD3-SD4 interface is translated to increased binding affinity, which drives increased biological activity.

The structural difference between the human and mouse IFNAR1 structures is consistent with the intrinsic mobility of IFNAR1

Encouraged from our success in resolving the conformational movements between unbound and bound IFNAR1, we aimed to rationalize the structural divide between the mouse and human IFNAR1 structures. Comparison of the structure modeled for human IFNAR1 (Thomas *et al.*, 2011) and that X-ray resolved for mouse IFNAR1 (de Weerd *et al.*, 2013) shows that the mouse structure assumes a more compact conformation, compared to the human (Fig. 7a). The RMSD between these respective *bent* and *extended* structures, after optimal superposition, is 10.2 Å. This difference is, to a large extent, due to the reorientation of SD4. We examined whether this structural difference between the human and mouse IFNAR1 can be explained by the global modes of motions encoded by the architecture, using the ANM. Movements along the ANM mode 1 for human IFNAR1 and mode 3 for mouse IFNAR1 were in fact found to reduce the RMSD between the two structures to 6.5 Å (Fig. 7b). Note that these motions are readily accessible via thermal fluctuations, and it is plausible that the human and mouse IFNAR1 adapt to different experimental conditions, functional states and/or sequence variations by simply reconfiguring along these soft directions of global movements (for a review see (Haliloglu and Bahar, 2015)).

We further performed MD simulations for human IFNAR1, which also confirmed the adaptability of the receptor to reconfigure from its original extended conformation to a bent form similar to the mouse structure, or to readily sample the conformational space between the human and mouse structures (see Fig. 7c). The distances between the two terminal subdomains SD1 and SD4 exhibited a significant change (from 107.4 to 86.6 Å using the same probe residues, N23 and T407) between the initial (*cyan*) and final (*violet*) conformations of the human IFNAR1. We note that the 268–328 disulfide bridge (see above) is only possible when modeling SD3 and SD4 as a gene duplication of SD1 and SD2. In the resolved mouse structure of IFNAR1 the C^{α}-distance between homologous positions to 268–328 in human is ~30 Å (Fig. 5a).

Assessing key interactions near the global hinge bending sites of IFNAR1

ANM analysis already revealed the major hinge sites that control the global movements of IFNAR1. The identity of key residues and interactions at these sites was further investigated by GNM analysis. Fig. 8 presents the results. Panel **A** displays the shapes of the two global modes. The crossover region between positive and negative movements along those axes define the global hinge centers: E199-N200 in mode 1 (*left*) and Q100 and Q302 in mode 2 (*right*). The former, E199-N200, at the crossover between positive and negative direction motions ($y = 0$ in the mode shape), is the *global hinge center* that defines the boundary between the two halves (respective pairs SD1-SD2 and SD3-SD4) of IFNAR1 which exhibit opposite-directions (anticorrelated) movements along mode 1 axis. Notably, the SD3 loop region K240-L247 shows a tendency to be coupled to the first half of the receptor (extremum near $y = 0$ in Fig. 8a). Likewise E111 and N290, neighboring the global hinge from both sides appear to be involved in the coupling of subdomains SD2 and SD3.

Similarly, mode 2 reveals the association of the SD2 loop T123-V127 with SD1 (or that D15 with SD2). We also note that the above cross-linked residues Q268 and Q328 are closely involved in the association of subdomains SD3 and SD4. Fig. 8b displays the locations of these residues implicated in inter-subdomain couplings along with their interacting (closest) partners across the neighboring subdomain. The figure also displays the pair I162-E293 (located on both sides of the global hinge) distinguished by large inter-residue distance fluctuations. Fig. 8c displays the fluctuations in IFNAR1 inter-residue distances, ΔR_{ij}, induced in the most collective motions. The *blue circles* highlight the sequentially distant (but spatially close) residue pairs that are distinguished by large *inter-subdomain* distance fluctuations (G133-F238 and L134-R241, in addition to I162-E293). Fig. S3 and Animations S5 and S6 show the inter-residue distance changes at these three pairs of residues. We postulated that interfering with these distance fluctuations, e.g. locking them by disulfide bridges, would interfere with mode 1, and thereby function of IFNAR1, in accord with the observed functional significance of global motions in other biomolecular systems (Bahar *et al.*, 2010). Next, we present the experimental verification of these predictions.

In vitro validation of the functional significance of key interactions between the different domains

To examine the functional significance of IFNAR1 conformational motions and their contribution to IFN-binding and receptor activation, we introduced a series of double-Cys mutants that would hinder inter-subdomain movements by forming disulfide bonds. Table 1 lists the double mutants constructed to this aim (see also Fig. 8b), and the distance between the residue pairs that have been replaced by cysteines based on the α-carbon coordinates in the human IFNAR1 (PDB id: **3S98** with modeled SD4).

We essentially selected two groups of residue pairs: (i) those identified above to potentially restrict the receptor global (SD2-SD3 interfacial) flexibility if cross-linked (set I in Table 1), and (ii) additional pairs that connect between the adjacent subdomains, mainly located in the close vicinity of the hinge center (set II). Five potential disulfide bridges where designed for restricting the flexibility at the SD2-SD3 hinge, and two for SD1-SD2 hinge. For all 8 mutant receptors, we measured binding of ^{125}I labeled IFNα2 (Fig. 9a and Table S1). The results show that 1.5 nM IFNα2 saturate the surface receptor for disulfide mutants bridging SD1-SD2 (*left*) and SD3-SD4 (*right*), while binding to most SD2-SD3 mutants (*middle*) is compromised. For three of the five disulfide bonds introduced between SD2 and SD3, almost complete loss of binding is observed (133–238, 134–241, 163–293); for two, a moderate loss was observed (111–290, 162–293). The different behavior of I162 and Y163, both of which form disulfide bridges with E293, can be easily explained by the opposite orientations of the side chains of these two consecutive residues on the β-strand, one (Y163) facing toward E293, and the other (I162) pointing away from E293 (see Fig. S4). The complete loss of ^{125}I IFNα2 surface binding observed in the double mutant Y163C-E293C, as opposed to the moderate loss in I162C-E293C, is consistent with their distinctive orientational predispositions to form cross-links with C293. The ability of IFNAR1 to bind IFNα2 is consistent with that expected from the relative positioning of these residue pairs with respect to the hinge center: essentially cross-linking those pairs with a larger torque (i.e. further away from the global hinge center E199) generally had a more restrictive effect on

inter-subdomain rotational flexibility, which in turn, compromised the optimal binding of IFNα2 (see Fig. 8b and Fig. S5). It should be noted however, that the disulfide-bridge forming residues G133, F238, L134 and R241 are located at the IFN-binding interface (see Table S2), and it is conceivable that modifications at those sites, and in particular, the cross-links (133–238 and 134–241) that restrict their conformational adaptability, would directly weaken the IFN-binding affinity.

Next, we measured EC50 values for IFI6 and MX1 gene induction (Fig. 9b and c), which is more sensitive than the surface IFN binding measurements. Here, we see a modest increase in IFNα2 EC50 values for 15–123 and 16–127 disulfide mutants and some decrease for the mutant Q268C-Q328C. Again, as with ^{125}I binding, the biggest increase in EC50 values are observed for the SD2-SD3 mutants, with the order of EC50 values (from large to small) being: 133–238 > 134–241 > 163–293 > 162–293 > 111–290. Note that the activity loss is in line with the loss in binding and the relative restrictive effects of these covalent bonds on IFNAR1 global hinge-bending.

A subset of 4 of these mutant receptors (15–123, 16–127, 111–290 and 163–293, in addition to 268–328) was expressed, purified and further investigated. The purified receptors were subjected to analytical gel filtration and SDS page without DTT to verify that they are monomers. In addition, the disulfide bond formation was verified by adding maleimide alexa flour 647 (see materials and methods). The binding affinity of IFNα2 and YNS-IFN to the purified receptors was determined by SPR (Figs. 9e, 10b, and S2 and Table S1). In addition, we determined the EC50 for antiviral activity of stably transfected cells with these 5 receptors and gene induction of a larger set of interferon induced representative genes using the fluidigm (Fig. 9d and 10a, and Table S1). The extended analysis shows moderately reduced binding and antiviral activity for the two SD1-SD2 mutations, a large decrease in antiviral activity for the SD2-SD3 mutant 163–293 and somewhat less decrease for 111–290. Using the fluidigm system to evaluate the induction of a wider set of genes by IFN verifies the results obtained for IFI6 and MX1 (Fig. 10a) and suggests that the results obtained for these two genes represents the gene induction by IFNα2 in Huh7 cells. Surprisingly, the binding affinity of IFNα2 and YNS as measured by SPR towards 111–290 was weaker than that measured for 163–293 (Fig. 9e, 10b, S2 and Table S1), in contradiction with all the cell surface results for these two mutant receptors. This would suggest an additional effect of 111–290 on ternary complex stability (including IFNAR2), which is not observed for IFNAR1 binding by itself.

Fig. 10b and Table S1 summarize the experimental results obtained for the different disulfide-bridge forming double mutants. The overall tendency is that disulfide bonds connecting SD2 to SD3 have the largest negative effect on IFN binding and signaling. The effect of SD1-SD2 disulfide mutations is moderate while connecting SD3 to SD4 seems to increase binding and activity. Overall, these results support the notion that dynamic modulation of the IFNAR1 receptor serves as a mechanism to affect binding affinity, which in turn is a mechanism to regulate interferon signaling.

Discussion

Originally, it was hypothesized that signal transduction by cytokines is a result of receptor dimerization, which initiates the intracellular associated kinases (Cunningham *et al.*, 1991; Sprang and Bazan, 1993). However, over time, more elaborate schemes for receptor activation have been proposed, involving pre-formed receptors that are activated by structural rearrangements. For example, it was suggested that both growth hormone and the EPO receptors exist as preformed dimers, with ligand-binding inducing structural changes transmitted to the IC domains (Livnah *et al.*, 1999; Brown *et al.*, 2005; Gadd and Clevenger, 2006). These findings were followed by studies of other cytokine receptors including IL6R, EGFR, VEGFR and IFNAR, where ligand-induced structural rearrangements of the IC domains were suggested to play an important role in signaling (Damjanovich *et al.*, 1997; Krause *et al.*, 2002, 2006a, 2006b; Tenhumberg *et al.*, 2006; Zaks-Zilberman *et al.*, 2008; Stuttfeld and Ballmer-Hofer, 2009; Krause *et al.*, 2013; Kavran *et al.*, 2014; Freed *et al.*, 2015). Also IFN binding was shown to result in conformational movements in IFNAR1, evident from comparing the unbound to bound structures of the ternary complex and from fluorescence quench and FRET studies (Strunk *et al.*, 2008a; Thomas *et al.*, 2011). However, the functional importance of IFNAR1 structural plasticity in modulating IFN signaling was not resolved.

In previous work, we have shown that even drastic changes in the transmembrane domain of IFNAR1 would not affect IFN binding affinity nor its induced activity (Sharma *et al.*, 2016). This would suggest that extracellular receptor plasticity is not transferred through the TM domain into the IC (mostly natively unstructured) domain of the receptor. Still, this did not resolve the functional role of receptor dynamics in this system. Here, we show that the intrinsic conformational dynamics of IFNAR1 permits the receptor to mediate its binding affinity to IFNs, which in turn modulates the IC signaling activity. This in turn opens new avenues for controlling functionality by altering receptor dynamics. We suggest this to be another layer of controlling receptor mediated signaling. The present study performed for IFNα2 also permits us to make inferences on other Type –I interferons. For example, IFNβ maintains the same overall fold, and shares the same binding interface with receptors IFNAR1 and IFNAR2 as does IFNα2 (Piehler et al., 2012); as such its global dynamics would be comparable to that of IFNα2, but the absolute binding affinity may differ due to its sequence specificity. The alteration of the dynamics of IFNAR1 could thus change the binding affinity of IFNβ qualitatively in the same direction as that shown for IFNα2, while the absolute strength of binding may be stronger. Comparison of the relative binding of IFN-YNS (which binds IFNAR1 even tighter than IFNβ) and IFNα2 to the different IFNAR1 mutants shows the same trend for both (Table S1) further validating that the dynamic alterations in IFNAR1 will have a similar effect on the different type I IFN subtypes.

Modulating the dynamics of proteins has been suggested before to affect activity, including in other protein-protein interactions. The most studied case is for ubiquitin, where conformational dynamics was suggested to control ubiquitin-deubiquitinase interactions and to influence *in vivo* signaling (Phillips *et al.*, 2013; Smith *et al.*, 2016). Kastritis et al. suggested that binding affinity of macromolecular interactions can be affected by their dynamics (Kastritis and Bonvin, 2013). For maltose binding by the maltose-binding protein,

a conformational selection model was suggested to explain the relation between dynamics and binding (Seo *et al.*, 2014). For intrinsically disordered proteins (IDPs) folding dynamics was suggested as a mean to regulate binding affinity (Shammas *et al.*, 2016). Here, using ANM/GNM and MD simulations we were able to decipher the most probable modes of movements of IFNAR1, showing that specific residues serve as inter-subdomain hinges. Our analysis also suggested the location of residue pairs which, upon substitution by cysteines and formation of disulfide bonds might potentially modulate inter-domain receptor dynamics, and hence interferon binding affinity and biological activity. We correctly predicted that the further from the hinge we restrict the movements between SD2 and SD3 through the introduction of covalent disulfide bridges, the stronger the effect on binding and activity (Fig. 10). This is due to the increased torque between the two subdomains inflicted by the additional covalent interaction, which tightens the hold on the conformational selection process. This effect may be further pronounced in the case of residues making interfacial contacts, such as 133–238 and 134–241.

It is important to emphasize that the different conformations stabilized by the engineered disulfide bridges are naturally visited by movements readily accessible to IFNAR1 in its unbound state. These pre-existing movements have been pointed in previous studies to facilitate ligand-binding (Tobi and Bahar, 2005; Meireles *et al.*, 2011) or protein-protein interactions (Bakan and Bahar, 2009). Thus, to some extent one could suggest that the disulfide bonds interfere with the conformational selection process for altering ligand-binding affinity. It should be noted that the results obtained for IFNAR1 cannot distinguish between the conformational selection and induced fit models for protein-binding (Monod *et al.*, 1965; Koshland *et al.*, 1966) or a mixture of both (Zhou, 2010).

In summary, we present in this manuscript a new concept for controlling cytokine signaling through modulation of receptor dynamics. We showed that by introducing disulfide bridges at specific locations, which affect domain movements, we can modulate the binding affinity of interferons, and through this, the activity. Linking the subdomains SD1 and SD2 of IFNAR1 had only relatively minor effects, while introducing disulfide bonds between subdomains SD2 and SD3 substantially impaired the conformational flexibility required for accommodating IFN binding and thus reduced binding, and activity. This highlights the functional role of the movements coordinated by the global hinge center E199-N200 in optimizing the binding of IFNs. The effect of cross-linking the subunits on both sides of this central hinge increased with the distance from the hinge, due to the added torque on the two domains. Conversely, covalently linking subdomains SD3 to SD4 resulted in increased binding affinity (particularly between residues 268–328) and biological activity. This cross-link was shown by MD simulations to favor an extended conformation of IFNAR1 EC domain, thus prompting the receptor to readily bind its ligand (IFN).

The sizeable dynamic flexibility of IFNAR1 also explained the difference in structure of the SD4 domain modeled from the human structure and verified by disulfide crosslinking data and fluorescence quench experiments and the mouse structure (de Weerd *et al.*, 2013), which has 50% sequence homology with the human receptor. Still, one cannot preclude that the different conformer stabilized in the bound form of mouse IFNAR1 is not (at least partially) responsible for the species specificity of IFNs, with the mouse ligand not binding or

activating the human receptor and *vice versa*. One exciting aspect of viewing the cytokine-receptor interactions as modulated by receptor dynamics is the potential to design allosteric effector molecules for these interactions, which will be able to control the strength of cytokine signaling.

Materials and Methods

Cell lines and antibodies

Human Huh7 IFNAR1 knockout cells (4βRC strain) were kindly provided by Uze Gilles (Université Montpellier, France). Monoclonal anti-IFNAR1-EC AA3 antibody was a gift from Biogene. G418 was purchased from Gibco.

Cloning and transfection

Mutations were introduced to EC and full length IFNAR1 sequence present on pBac and pDisplay plasmids by PCR amplification with mismatch containing primers. Human hepatocarcinoma cell line Huh7 (IFNAR1 knockout cells 4βRC strain) was cultured at 37°C with 5% CO2 in DMEM (Sigma-Aldrich) supplemented with 10% fetal bovine serum (Equitech-BIO. Inc.), 1× penicillin-streptomycin-glutamine (Bio Labs). The cDNA-IFNAR1 with mutation in pDisplay plasmids were transiently transfected to Huh7 IFNAR1 knockout cells (4βRC strain) using Jet PEI following the manufacturer standard protocol.

Protein Expression and Purification

Mutated IFNAR1-EC sequences in pBAC3 plasmid were transfected to insect SF9 cells using cellfectine II along with the BaculoGold. Proteins used in this study were expressed as C-terminally his-tagged constructs and were secreted by Hi-5 cells. Proteins were purified using Nickel beads followed by size exclusion chromatography.

Analysis of IFNAR1 mutants

The size and folded state of the 5 expressed and purified IFNAR1 mutants (plus control wild-type) was verified by SDS page electrophoresis without DTT in the loading buffer (to probe for inter-protein disulfide bonds) and analytical gel filtration on a Superdex 200 column (GE). The six proteins were observed as single bands in the SDS gel. They eluted at 14.6±0.2 mL. To verify the formation of disulfide bonds in these proteins we used maleimide derivative alexa-flour 647 with extinction coefficient of 265,000 $cm^{-1}M^{-1}$ (ThermoFisher), added 10x excess of the dye to protein and incubated at 4°C ON. The excess dye was removed and absorbance at 280 and 647 nm were measured. The extinction coefficient of IFNAR1 is 85300 $cm^{-1}M^{-1}$. The molar ratios of 2xAlexa Flour/IFNAR1 for the 5 IFNAR1 disulfide mutants 15–123, 16–127, 163–293, 111–290 and 268–328 were 0.1, 0.35, 0.1, 0.25 and 0.1 respectively. These results suggest that the disulfide bridge being formed in all 5-cases.

Preparation of stable cell line

The different IFNAR1 mutants in pDisplay vector were transfected in Huh7 cell and were kept for selection (800 microgram/ml) with G418. IFNAR1-positive cells were sorted using

fluorescence activated cell sorter. In brief transfected Huh7 cell were wash with cold PBS and resuspended in PBS containing 1% BSA and incubate with AA3 antibody for one hour on ice followed by incubation with APC. Surface IFNAR1 levels were detected by the level of allophycocyanin (APC) values and cell expressing IFNAR1 were collected using FACSAria (BD).

In vitro binding assay

The mutant and wild type IFNs binding affinity towards IFNAR1-EC and IFNAR2-EC were determined by SPR, using the ProteOn XPR36, as detailed previously (Levin *et al.*, 2011). The dissociation constant K_D was obtained from the equilibrium response and the association and dissociation rate constants from 6 different analyte concentrations as previously described (Levin *et al.*, 2011).

Gene induction assay

Huh7 cells transfected with IFNAR1 receptors were treated with IFNs for sixteen hours. RNA were extracted with the PerfectPure RNA cultured cell kit (5 Prime) followed by cDNA preparation using high-capacity cDNA reverse transcription kit (Applied Biosystems). Selected human interferon-stimulated gene expression levels were measured with the ABI Prism 7300 real-time PCR system, using the SYBR green PCR master mix (Applied Biosystems). Expression fold-change of selected genes are displayed as $2^{-\Delta\Delta CT}$ values, with the HPRT1 gene being used as internal control. High-throughput qPCR was performed with BioMark 48 × 48 and 96 × 96 Dynamic Arrays (Fluidigm Corporation) according to the manufacturer's protocol. cDNAs (50 ng/ml) were preamplified with all the primers together and analyzed with the BioMark real-time PCR instrument. Initial data analysis was performed with the Fluidigm real-time PCR analysis software.

In situ binding assay

Wild-type IFNα2 was labeled with ^{125}I as described (Jacobs *et al.*, 1979). In brief, IFNα2 was labeled with ^{125}I using the chloramine T iodination method, and the radiolabeled ligand was passed through Sephadex-G10 size exclusion column. Stable and transiently transfected Huh7 cells were seeded for 24 h. The cells were washed once with PBS + 0.1% sodium azide, and then incubated for 10 min with the same solution. Next, cells were incubated for 1 h at room temperature with the labeled wild type IFNα2 (200,000 cpm/well) in the presence of an unlabeled IFNα2 at ten different concentrations from 200 nM at 4-fold dilution steps in culture medium + 0.1% sodium azide. Cells were then washed five times with PBS on ice to get rid of unbound interferons, Cells were removed from wells by using 0.1 M NaOH plus 0.1% SDS and transferred into test tubes for measuring of bound ^{125}I labeled IFNα2, using a γ-counter (Packard). The experiments were repeated three times, each time in duplicates. IC50 values were calculated using Kaleidagraph Synergy Software version 4.1.

Antiviral assays

$1.2\times10^4$of Huh7 cells expressing different mutant of IFNAR1 were grown on flat-bottomed 96-well plates overnight. Cells were treated with serial dilutions of IFNα2 for four hour and added EMCV. Cell survival curve were assessed after 14hr using crystal violet. The EC50

values to the indicated IFNs were determined from IFN dose-response curves, as previously described (Piehler *et al.*, 2000).

Mass spectrometry

Samples were re-suspended in 100mM Ammonium Bicarbonate to a final volume of 50ul. Samples were immediately digested with Chymotrypsin (Roche) without reduction and alkylation steps. Enzymatic digestion was carried out overnight at 25°C with Chymotrypsin at a ratio of 1:50 enzyme to protein (wt/wt.) 5ul of the resulting peptide mixtures were applied to a 15 cm reversed-phase fused-silica capillary column (inner diameter, 75 um) packed with 3 um ReproSil-Pur C18AQ media (Dr. Maisch GmbH). The LC system, an UltiMate 3000 (Dionex) was used in conjunction with an LTQ Orbitrap XL (Thermo Fisher Scientific) operated in the positive ion mode. Peptides were separated with a four-hour gradient from 5 to 65% acetonitrile (buffer A, 5% acetonitrile, 0.1% formic acid and 0.005% TFA; buffer B, 90% acetonitrile, 0.2% formic acid and 0.005%TFA). The voltage applied to the union to produce an electrospray was 1.2 kV. The seven most intense ions per scan were fragmented and analyzed in the linear ion trap. Data analysis was done with MassMatrix using disulfide exploratory search parameters.

Fluorescence quenching

ATTO 655 maleimide was purchased from ATTO-Tec (Siegen, Germany). The EC domains of IFNAR1 WT and SD34 mutant (both including the N349C mutation) were fused to an N-terminal decahistidine tag. The proteins were expressed in Sf9 insect cells using baculovirus infection and purified by immobilized metal-chelating chromatography as previously described. Proteins were labeled with ATTO655 as detailed in reference (Strunk *et al.*, 2008a). The labeling efficiency was 0.4–0.7 fluorophores per IFNAR1-H10 molecule for the purified proteins. Fluorescence dequenching in solution were carried out with 100 nM of fluorescence-labeled IFNAR1-EC supplemented with 1 mg/ml bovine serum albumin using 120-µl cuvette (Hellma) in Cary Eclipse (Varian) at 20 °C. Labeled proteins were excited at 640 nm and the emission between 660 and 800 nm was recorded.

GNM and ANM analyses

GNM and ANM analyses were performed using the *ProDy* API (Bakan *et al.*, 2011). GNM was used for evaluating the global hinge sites following the protocol described previously (Yang and Bahar, 2005). Briefly, structural coordinates are used to construct the Kirchhoff/connectivity matrix Γ, the eigenvalue decomposition of which yields a series of N-1 modes for a structure of N residues. The lowest-frequency (smallest eigenvalue) modes (eigenvectors), also called the *softest modes* define the most cooperative/global motions intrinsically accessible to the structure. The size and direction of residue motions along these modes (shown for modes 1 and 2 in Fig. 8a) reflect the relative mobilities of residues in the most cooperative movements, as well as the identity of hinge/anchor sites (at y = 0). The diagonal elements of the pseudoinverse Γ^{-1} scale with the mean-square fluctuations (MSFs) $\langle(\Delta R_i)^2\rangle$ of residues ($1 \le i \le N$), and the off-diagonal terms with their cross-correlations $\langle \Delta \mathbf{R}_i . \Delta \mathbf{R}_j \rangle$. These are used for evaluating the fluctuations in *inter-residue distances* $\langle(\Delta R_{ij})^2\rangle = \langle(\Delta \mathbf{R}_j - \Delta \mathbf{R}_i)^2\rangle = \langle(\Delta R_i)^2\rangle + \langle(\Delta R_j)^2\rangle - 2\langle \Delta \mathbf{R}_i . \Delta \mathbf{R}_j \rangle$, displayed in Fig. 8c.

ANM was used for evaluating the movements as functions of residue index *i*, for normal mode *k*, following the protocol described in our previous work, with cutoff distance of 15 Å (Eyal *et al.*, 2015). Computations in the presence of membrane were performed using the explicit *MembrANM* module in *ProDy*. Details of the method can be found in earlier work (Lezon and Bahar, 2012).

MD simulations

MD simulations were performed using NAMD 2.11 (Phillips *et al.*, 2005) with standard protocols, mainly NPT systems (300 K and 1 atm) with periodic boundary conditions, CHARMM36 force field and 2 fs time steps. All data refer to at least two independent runs performed for verifying the reproducibility of the results. MD simulations provide information complementary to that obtained from ANM analysis. ANM accurately predicts global dynamics and cooperative events, but residue-specific analyses are beyond the scope of ANM, as ANM is exclusively based on contact topology. MD simulations, on the other hand, provide information on specific interactions, especially on a local scale. Here, the effect of mutations, and motions at atomic scale were investigated using MD. Furthermore, the global motions inferred from MD trajectories were verified to be consistent with ANM global modes.

Error calculations

All the experiments were done using multiple biological replicates. The standard deviation for each type of experiment was calculated from all the available data of the same experiment. For example, the standard deviation for qPCR per gene was calculated from all the mutant data combined, assuming that the standard deviation is the same for the different mutants. The reason for this is that the different mutants were measured using the same method, and thus their respective standard deviation is expected to be the same. Indeed, the individual errors of each mutant measured in biological triplicates have a Gaussian distribution around an average, which represents a better estimate of the overall standard deviation than obtained for the individual mutant as the sample size is much larger. Standard deviation for EC50 of gene induction was 20%, for KD determined by SPR for YNS 25% and for IFNα2 33% and for EC50 for antiviral activity 33% of the measured values. Therefore, 95% significance between wild-type and mutant data requires differences of 55%, 70% and 90% respectively between them.

Supplementary Material

Refer to Web version on PubMed Central for supplementary material.

Acknowledgments

We want to thank Tevie Mehlman from the life science core facility, Weizmann Institute for the mass spectrometry work. This work was supported by United States-Israel Binational Science Foundation Grant 2011093, the European Community 7th Framework Program TRANSPOL, 264399, and the NIH grants P41 GM103712 and R01 GM099738.

References

Atilgan AR, Durell SR, Jernigan RL, Demirel MC, Keskin O, Bahar I. Anisotropy of fluctuation dynamics of proteins with an elastic network model. Biophys J. 2001; 80:505–515. [PubMed: 11159421]

Bahar I, Atilgan AR, Erman B. Direct evaluation of thermal fluctuations in proteins using a single-parameter harmonic potential. Fold Des. 1997; 2:173–181. [PubMed: 9218955]

Bahar I, Lezon TR, Yang LW, Eyal E. Global dynamics of proteins: bridging between structure and function. Annu Rev Biophys. 2010; 39:23–42. [PubMed: 20192781]

Bakan A, Bahar I. The intrinsic dynamics of enzymes plays a dominant role in determining the structural changes induced upon inhibitor binding. Proc Natl Acad Sci U S A. 2009; 106:14349–14354. [PubMed: 19706521]

Bakan A, Meireles LM, Bahar I. ProDy: protein dynamics inferred from theory and experiments. Bioinformatics. 2011; 27:1575–1577. [PubMed: 21471012]

Brierley MM, Fish EN. Review: IFN-alpha/beta receptor interactions to biologic outcomes: understanding the circuitry. J Interferon Cytokine Res. 2002; 22:835–845. [PubMed: 12396722]

Brown RJ, Adams JJ, Pelekanos RA, Wan Y, McKinstry WJ, Palethorpe K, Seeber RM, Monks TA, Eidne KA, Parker MW, Waters MJ. Model for growth hormone receptor activation based on subunit rotation within a receptor dimer. Nat Struct Mol Biol. 2005; 12:814–821. [PubMed: 16116438]

Cunningham BC, Ultsch M, De Vos AM, Mulkerrin MG, Clauser KR, Wells JA. Dimerization of the extracellular domain of the human growth hormone receptor by a single hormone molecule. Science. 1991; 254:821–825. [PubMed: 1948064]

Damjanovich S, Bene L, Matko J, Alileche A, Goldman CK, Sharrow S, Waldmann TA. Preassembly of interleukin 2 (IL-2) receptor subunits on resting Kit 225 K6 T cells and their modulation by IL-2, IL-7, and IL-15: a fluorescence resonance energy transfer study. Proc Natl Acad Sci U S A. 1997; 94:13134–13139. [PubMed: 9371812]

de Weerd NA, Vivian JP, Nguyen TK, Mangan NE, Gould JA, Braniff SJ, Zaker-Tabrizi L, Fung KY, Forster SC, Beddoe T, Reid HH, Rossjohn J, Hertzog PJ. Structural basis of a unique interferon-beta signaling axis mediated via the receptor IFNAR1. Nat Immunol. 2013; 14:901–907. [PubMed: 23872679]

Eyal E, Lum G, Bahar I. The anisotropic network model web server at 2015 (ANM 2.0). Bioinformatics. 2015; 31:1487–1489. [PubMed: 25568280]

Foster GR, Masri SH, David R, Jones M, Datta A, Lombardi G, Runkell L, de Dios C, Sizing I, James MJ, Marelli-Berg FM. IFN-alpha subtypes differentially affect human T cell motility. J Immunol. 2004; 173:1663–1670. [PubMed: 15265895]

Freed DM, Alvarado D, Lemmon MA. Ligand regulation of a constitutively dimeric EGF receptor. Nat Commun. 2015; 6:7380. [PubMed: 26060020]

Gadd SL, Clevenger CV. Ligand-independent dimerization of the human prolactin receptor isoforms: functional implications. Mol Endocrinol. 2006; 20:2734–2746. [PubMed: 16840534]

Haliloglu T, Bahar I. Adaptability of protein structures to enable functional interactions and evolutionary implications. Curr Opin Struct Biol. 2015; 35:17–23. [PubMed: 26254902]

Jacobs S, Hazum E, Shechter Y, Cuatrecasas P. Insulin receptor: covalent labeling and identification of subunits. Proc Natl Acad Sci U S A. 1979; 76:4918–4921. [PubMed: 291908]

Jaitin DA, Roisman LC, Jaks E, Gavutis M, Piehler J, Van der Heyden J, Uze G, Schreiber G. Inquiring into the differential action of interferons (IFNs): an IFN-alpha2 mutant with enhanced affinity to IFNAR1 is functionally similar to IFN-beta. Mol Cell Biol. 2006; 26:1888–1897. [PubMed: 16479007]

Jaks E, Gavutis M, Uze G, Martal J, Piehler J. Differential receptor subunit affinities of type I interferons govern differential signal activation. J Mol Biol. 2007; 366:525–539. [PubMed: 17174979]

Kalie E, Jaitin DA, Abramovich R, Schreiber G. An Interferon {alpha}2 Mutant Optimized by Phage Display for IFNAR1 Binding Confers Specifically Enhanced Antitumor Activities. J Biol Chem. 2007; 282:11602–11611. [PubMed: 17310065]

Kalinke U, Prinz M. Endogenous, or therapeutically induced, type I interferon responses differentially modulate Th1/Th17-mediated autoimmunity in the CNS. Immunol Cell Biol. 2012

Kastritis PL, Bonvin AM. On the binding affinity of macromolecular interactions: daring to ask why proteins interact. J R Soc Interface. 2013; 10:20120835. [PubMed: 23235262]

Kavran JM, McCabe JM, Byrne PO, Connacher MK, Wang Z, Ramek A, Sarabipour S, Shan Y, Shaw DE, Hristova K, Cole PA, Leahy DJ. How IGF-1 activates its receptor. Elife. 2014:3.

Koshland DEJ, Nemethy G, Filmer D. Comparison of experimental binding data and theoretical models in proteins containing subunits. Biochemistry. 1966; 5:365–385. [PubMed: 5938952]

Kotenko SV, Langer JA. Full house: 12 receptors for 27 cytokines. Int Immunopharmacol. 2004; 4:593–608. [PubMed: 15120645]

Krause CD, Digioia G, Izotova LS, Xie J, Kim Y, Schwartz BJ, Mirochnitchenko OV, Pestka S. Ligand-independent interaction of the type I interferon receptor complex is necessary to observe its biological activity. Cytokine. 2013; 64:286–297. [PubMed: 23830819]

Krause CD, Lavnikova N, Xie J, Mei E, Mirochnitchenko OV, Jia Y, Hochstrasser RM, Pestka S. Preassembly and ligand-induced restructuring of the chains of the IFN-gamma receptor complex: the roles of Jak kinases, Stat1 and the receptor chains. Cell Res. 2006a; 16:55–69. [PubMed: 16467876]

Krause CD, Mei E, Mirochnitchenko O, Lavnikova N, Xie J, Jia Y, Hochstrasser RM, Pestka S. Interactions among the components of the interleukin-10 receptor complex. Biochem Biophys Res Commun. 2006b; 340:377–385. [PubMed: 16364239]

Krause CD, Mei E, Xie J, Jia Y, Bopp MA, Hochstrasser RM, Pestka S. Seeing the light: preassembly and ligand-induced changes of the interferon gamma receptor complex in cells. Mol Cell Proteomics. 2002; 1:805–815. [PubMed: 12438563]

Lavoie TB, Kalie E, Crisafulli-Cabatu S, Abramovich R, Digioia G, Moolchan K, Pestka S, Schreiber G. Binding and activity of all human alpha interferon subtypes. Cytokine. 2011; 56:282–289. [PubMed: 21856167]

Levin D, Harari D, Schreiber G. Stochastic Receptor Expression Determines Cell Fate upon Interferon Treatment. Mol Cell Biol. 2011; 31:3252–3266. [PubMed: 21690295]

Levin D, Schneider WM, Hoffmann HH, Yarden G, Busetto AG, Manor O, Sharma N, Rice CM, Schreiber G. Multifaceted activities of type I interferon are revealed by a receptor antagonist. Sci Signal. 2014; 7:ra50. [PubMed: 24866020]

Lezon TR, Bahar I. Constraints imposed by the membrane selectively guide the alternating access dynamics of the glutamate transporter GltPh. Biophys J. 2012; 102:1331–1340. [PubMed: 22455916]

Li H, Chang YY, Yang LW, Bahar I. iGNM 2.0: the Gaussian network model database for biomolecular structural dynamics. Nucleic Acids Res. 2016; 44:D415–22. [PubMed: 26582920]

Livnah O, Stura EA, Middleton SA, Johnson DL, Jolliffe LK, Wilson IA. Crystallographic evidence for preformed dimers of erythropoietin receptor before ligand activation. Science. 1999; 283:987–990. [PubMed: 9974392]

Marijanovic Z, Ragimbeau J, van der Heyden J, Uze G, Pellegrini S. Comparable potency of IFNalpha2 and IFNbeta on immediate JAK/STAT activation but differential down-regulation of IFNAR2. Biochem J. 2007; 407:141–151. [PubMed: 17627610]

Meireles L, Gur M, Bakan A, Bahar I. Pre-existing soft modes of motion uniquely defined by native contact topology facilitate ligand binding to proteins. Protein Sci. 2011; 20:1645–1658. [PubMed: 21826755]

Monod J, Wyman J, Changeux JP. On the nature of allosteric transitions: a plausible model. J Mol Biol. 1965; 12:88–118. [PubMed: 14343300]

Novick D, Cohen B, Rubinstein M. The human interferon alpha/beta receptor: characterization and molecular cloning. Cell. 1994; 77:391–400. [PubMed: 8181059]

Phillips AH, Zhang Y, Cunningham CN, Zhou L, Forrest WF, Liu PS, Steffek M, Lee J, Tam C, Helgason E, Murray JM, Kirkpatrick DS, Fairbrother WJ, Corn JE. Conformational dynamics control ubiquitin-deubiquitinase interactions and influence in vivo signaling. Proc Natl Acad Sci U S A. 2013; 110:11379–11384. [PubMed: 23801757]

Phillips JC, Braun R, Wang W, Gumbart J, Tajkhorshid E, Villa E, Chipot C, Skeel RD, Kale L, Schulten K. Scalable molecular dynamics with NAMD. J Comput Chem. 2005; 26:1781–1802. [PubMed: 16222654]

Piehler J, Roisman LC, Schreiber G. New structural and functional aspects of the type I interferon-receptor interaction revealed by comprehensive mutational analysis of the binding interface. J Biol Chem. 2000; 275:40425–40433. [PubMed: 10984492]

Piehler J, Thomas C, Christopher Garcia K, Schreiber G. Structural and dynamic determinants of type I interferon receptor assembly and their functional interpretation. Immunol Rev. 2012; 250:317–334. [PubMed: 23046138]

Platanias LC. Mechanisms of type-I- and type-II-interferon-mediated signalling. Nat Rev Immunol. 2005; 5:375–386. [PubMed: 15864272]

Schreiber G, Piehler J. The molecular basis for functional plasticity in type I interferon signaling. Trends Immunol. 2015; 36(3):139–149. [PubMed: 25687684]

Seo MH, Park J, Kim E, Hohng S, Kim HS. Protein conformational dynamics dictate the binding affinity for a ligand. Nat Commun. 2014; 5:3724. [PubMed: 24758940]

Severa M, Remoli ME, Giacomini E, Ragimbeau J, Lande R, Uze G, Pellegrini S, Coccia EM. Differential responsiveness to IFN-alpha and IFN-beta of human mature DC through modulation of IFNAR expression. J Leukoc Biol. 2006; 79:1286–1294. [PubMed: 16624932]

Shammas SL, Crabtree MD, Dahal L, Wicky BI, Clarke J. Insights into Coupled Folding and Binding Mechanisms from Kinetic Studies. J Biol Chem. 2016; 291:6689–6695. [PubMed: 26851275]

Sharma N, Longjam G, Schreiber G. Type I Interferon Signaling Is Decoupled from Specific Receptor Orientation through Lenient Requirements of the Transmembrane Domain. J Biol Chem. 2016; 291:3371–3384. [PubMed: 26679999]

Smith CA, Ban D, Pratihar S, Giller K, Paulat M, Becker S, Griesinger C, Lee D, de Groot BL. Allosteric switch regulates protein-protein binding through collective motion. Proc Natl Acad Sci U S A. 2016; 113:3269–3274. [PubMed: 26961002]

Sprang SR, Bazan JF. Cytokine structural taxonomy and mechanisms of receptor engagement. Curr Opin Struct Biol. 1993; 3:815–827.

Stark GR, Darnell JEJ. The JAK-STAT Pathway at Twenty. Immunity. 2012; 36:503–514. [PubMed: 22520844]

Strunk JJ, Gregor I, Becker Y, Lamken P, Lata S, Reichel A, Enderlein J, Piehler J. Probing Protein Conformations by in Situ Non-Covalent Fluorescence Labeling. Bioconjug Chem. 2008a; 20:41–46.

Strunk JJ, Gregor I, Becker Y, Li Z, Gavutis M, Jaks E, Lamken P, Walz T, Enderlein J, Piehler J. Ligand binding induces a conformational change in ifnar1 that is propagated to its membrane-proximal domain. J Mol Biol. 2008b; 377:725–739. [PubMed: 18294654]

Stuttfeld E, Ballmer-Hofer K. Structure and function of VEGF receptors. IUBMB Life. 2009; 61:915–922. [PubMed: 19658168]

Tenhumberg S, Schuster B, Zhu L, Kovaleva M, Scheller J, Kallen KJ, Rose-John S. gp130 dimerization in the absence of ligand: preformed cytokine receptor complexes. Biochem Biophys Res Commun. 2006; 346:649–657. [PubMed: 16774741]

Thomas C, Moraga I, Levin D, Krutzik PO, Podoplelova Y, Trejo A, Lee C, Yarden G, Vleck SE, Glenn JS, Nolan GP, Piehler J, Schreiber G, Garcia KC. Structural Linkage between Ligand Discrimination and Receptor Activation by Type I Interferons. Cell. 2011; 146:621–632. [PubMed: 21854986]

Tobi D, Bahar I. Structural changes involved in protein binding correlate with intrinsic motions of proteins in the unbound state. Proc Natl Acad Sci U S A. 2005; 102:18908–18913. [PubMed: 16354836]

Uze G, Schreiber G, Piehler J, Pellegrini S. The receptor of the type I interferon family. Curr Top Microbiol Immunol. 2007; 316:71–95. [PubMed: 17969444]

Yang LW, Bahar I. Coupling between catalytic site and collective dynamics: a requirement for mechanochemical activity of enzymes. Structure. 2005; 13:893–904. [PubMed: 15939021]

Zaks-Zilberman M, Harrington AE, Ishino T, Chaiken IM. Interleukin-5 receptor subunit oligomerization and rearrangement revealed by fluorescence resonance energy transfer imaging. J Biol Chem. 2008; 283:13398–13406. [PubMed: 18326494]

Zhou HX. From induced fit to conformational selection: a continuum of binding mechanism controlled by the timescale of conformational transitions. Biophys J. 2010; 98:L15–7. [PubMed: 20303846]

Highlights

- Interferon mediated receptor dimerization of IFNAR1 and IFNAR2 dictates signaling
- The inherent flexibility of IFNAR1 enables it to probe multiple conformations
- Restricting IFNAR1 conformational space affects its interferon binding and activity
- Dynamic modulation serves as a mechanism for regulating cytokine signaling

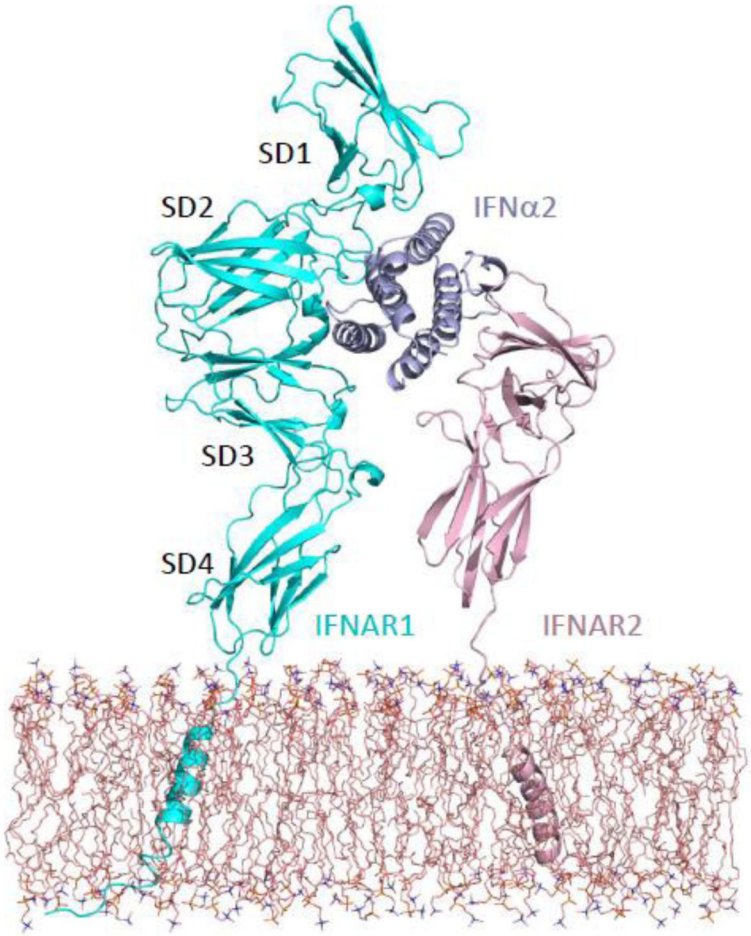

Fig. 1. Heterotrimeric complex of IFNa2, IFNAR1 and IFNAR2 in the presence of lipid bilayer

The structure is composed of the experimentally resolved complex (PDB id: **3SE3**) comprised of IFNAR1 EC subdomains SD1–3, IFNα2 and IFNAR2, the IFNAR1-SD4 domain, and two transmembrane (TM) helices at the C-termini of the receptors, embedded into a POPC lipid bilayer constructed *in silico*.

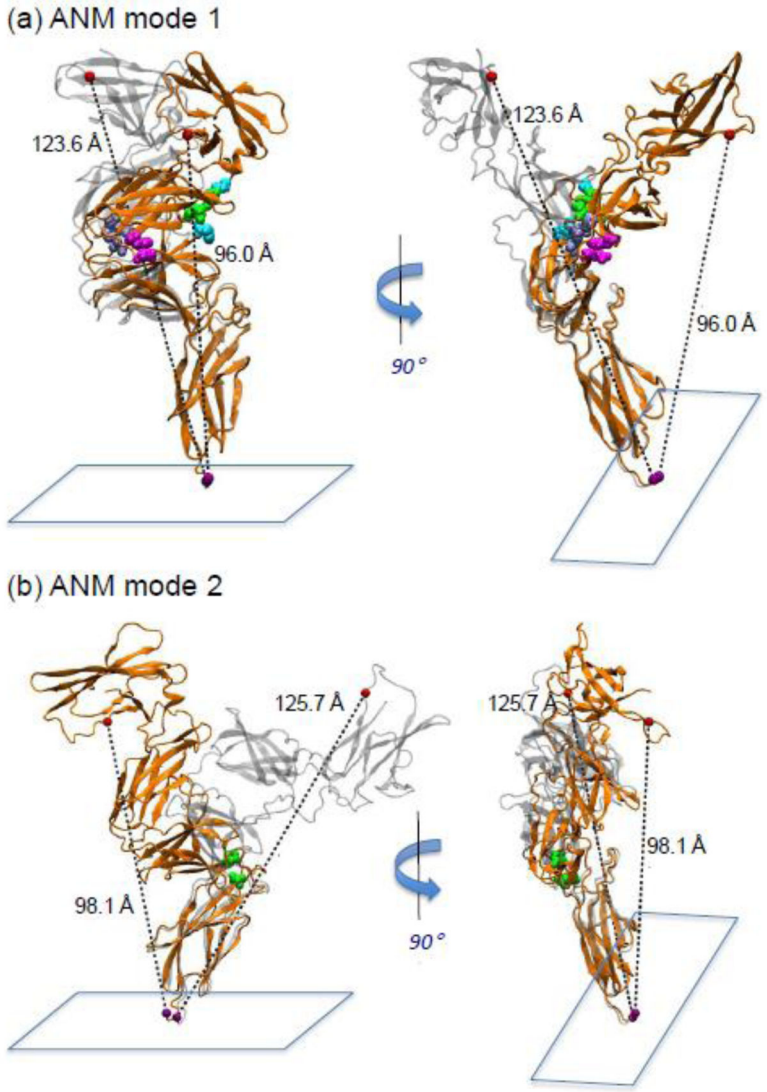

Fig. 2. Conformational flexibility of IFNAR1 EC domain

Each panel shows two conformations, compact/bent (*orange)* and extended (*gray*) sampled upon global fluctuations along the modes 1 (**a**) and 2 (**b**). The *left* and *right* panels display the front and side views. Mode 1 involves a bending around a central hinge at the interface between SD2 and SD3; Mode 2 induces an orthogonal bending by flexing at SD3-SD4 interfacial hinge center. The decrease in the distance between N23 on SD1 (*red sphere*) and T407 on SD4 (*magenta*) in the bent forms is consistent with that observed in FRET experiments [21]. Residue pairs making SD2-SD3 inter-subdomain contacts, G133-F238, L134-R241, Y163-E293 and E111-F290, are shown by *cyan*, *green*, *magenta* and *blue/gray* spheres, respectively in (**a**). The SD3-SD4 interfacial pair, Q268-Q328, is colored *green* in (**b**); see also the respective Animation 1 and 2.

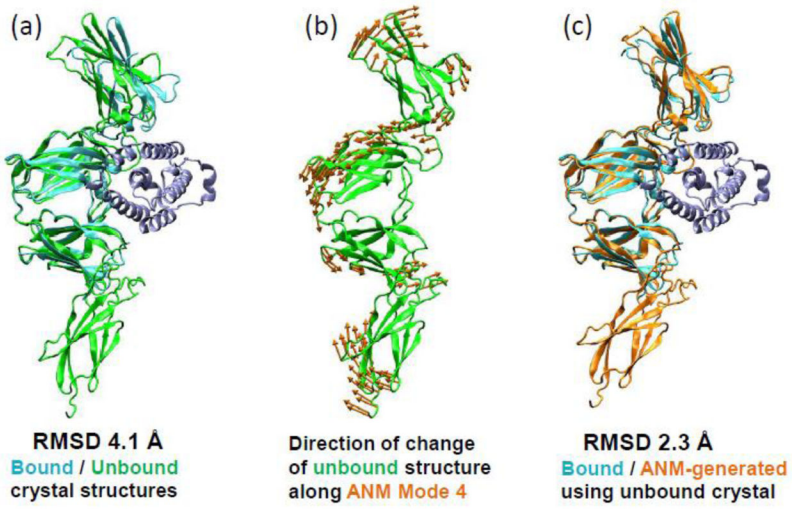

Fig. 3. Intrinsic ability of IFNAR1 structure to adapt to functional interactions

The change observed experimentally between the unbound (*green*) and bound (*cyan*) structures of IFNAR1 agrees with the changes intrinsically favored by ANM global modes. The conformer colored *orange* is obtained upon moving the unbound form (*green*) along a global ANM mode (ANM mode 4). See also Animation 3. This conformer resembles that of the bound IFNAR1 (*cyan*), indicating that the receptor (unbound) structure favors this functional change in conformation (i.e., unbound IFNAR1 is predisposed to take on the bound conformation). The RMSD between the experimentally resolved unbound and bound forms is 4.1 Å; that between the ANM-driven conformer and experimentally resolved bound form is 2.3 Å, i.e. the movement along mode 4 helps the unbound IFNAR1 move toward the conformation that is stabilized upon binding the substrate (IFNα2).

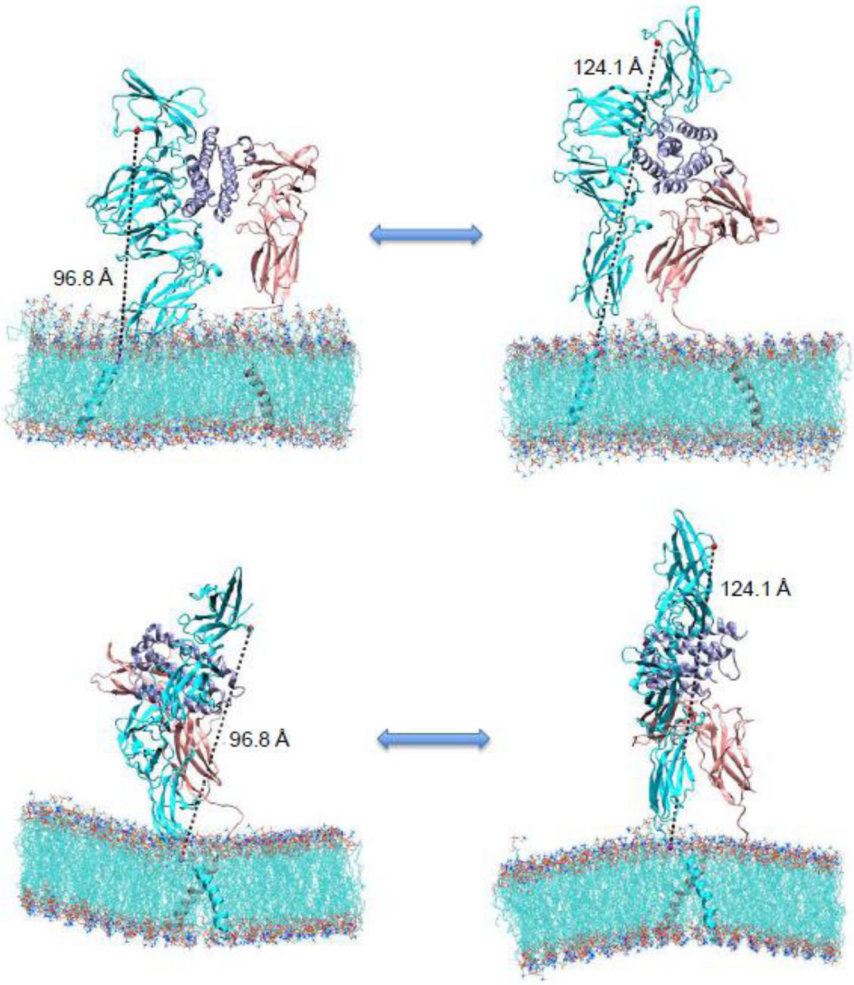

Fig. 4. IFNAR1 ternary complex attached to the membrane retains its adaptability to functional interactions

Global fluctuations of ternary complex formed by IFNAR1, IFNa2 and IFNAR2 (colored *cyan*, *light violet* and *pink*, respectively) modeled in the presence of lipid bilayer. The left and right diagrams display alternative conformations. The lower two diagrams display the same conformations, from a different perspective (90° rotation around the vertical axis). The distance between N23 (*red sphere*) and T407 (*magenta sphere*) decreases by ~10 Å in bent conformation with respect to the starting conformer; see also Animation 4.

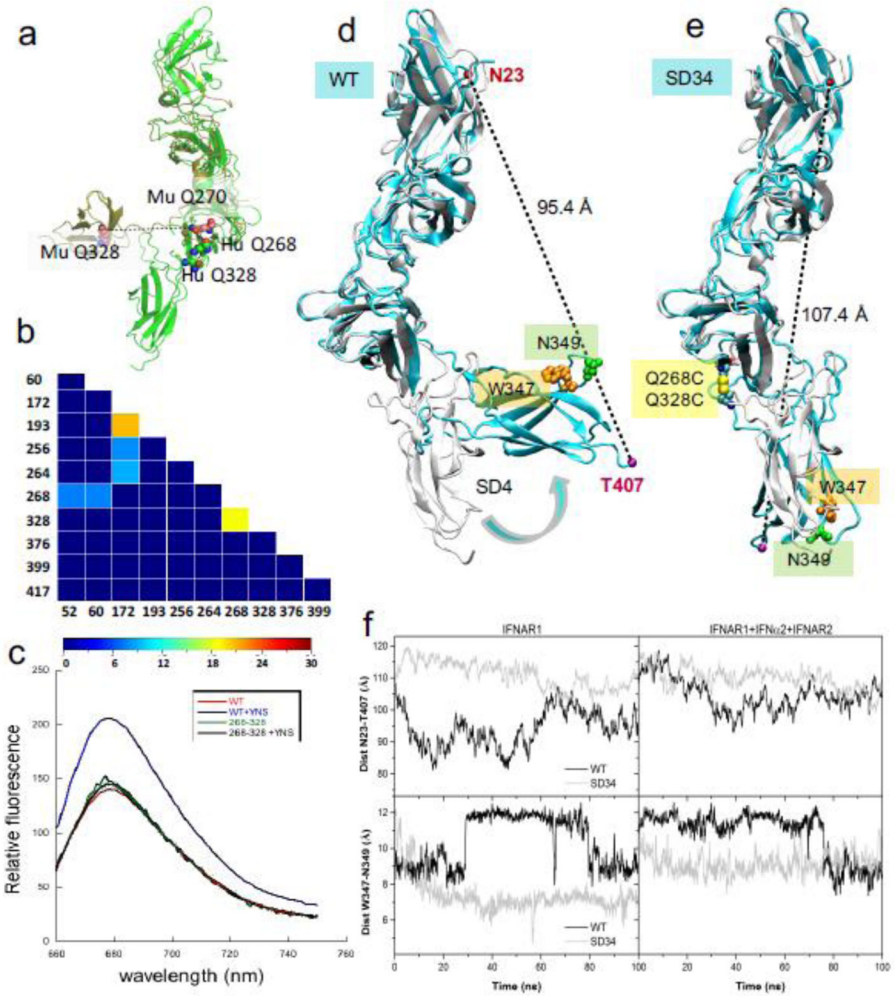

Fig. 5. Formation of a disulfide bridge in the mutant Q268C-Q328C, and its effect on IFNAR1 structure and dynamics

(a) Overlay of human (*green*) and mouse (*tan*) IFNAR1. Residues 268 and 328, shown in CPK space filling, are within disulfide bridge-forming distance in the human, and the homologous positions are ~30 Å apart in the mouse. **(b)** Disulfide bridge 268C-328C detected by mass spectrometry. The purified receptor was digested with chymotrypsin as described in Materials and Methods, and subjected to MS analysis. The resulting mass data searched with MassMatrix indicates that 193–172 and 268–328 form disulfide bonds (color code from *blue* (no disulfide) to *red* (high confidence disulfide)). The data are a representative of one of the two independent experiments done. **(c)** Monitoring SD4 movement by electron transfer from a fluorescence dye (AT655) covalently bonded to residue N349C. Fluorescence quenching by neighboring W347 is abrogated upon IFN binding. No abrogation of quenching is observed in Q268C-Q328C double mutant, suggesting that the latter does not undergo (upon IFN binding) a conformational change that affects the relative positions of N349 and W347. The data shown are a representative of one of the three independent experiments done. **(d)** and **(e)** MD trajectories generated for IFNAR1-IFNa2-IFNAR2 using wild-type and double mutant Q268C-Q328C IFNAR1,

shortly designated as WT and SD34. SD4 movement is severely restricted in SD34 **(e)** compared to the WT **(d).** The diagrams show the initial IFNAR1 conformation (*white*) and its 40th ns snapshots (*cyan*) in the presence of IFN and IFNAR2 (not shown for clarity). During the course of simulations SD1-SD4 distance is reduced by more than 10 Å in the WT; whereas it remains unchanged in the double mutant. The positions of W347 and N349 are shown in both cases. **(f)** *(top*) Time evolution of the C^{a} distances between N23 (SD1) and T407 (SD4) in the simulations of IFNAR1 (*left*) and the ternary complex (IFNAR1+IFNa2+IFNAR2) (*right*). The original distance of 107 Å fluctuates in the range 85–115 Å approximately, in the WT; whereas it is confined to a narrower range, 105–115 Å, in SD34. (*bottom*) W347-N349 distance increases up to 12 Å in the WT; whereas it remains < 10 Å in SD34.

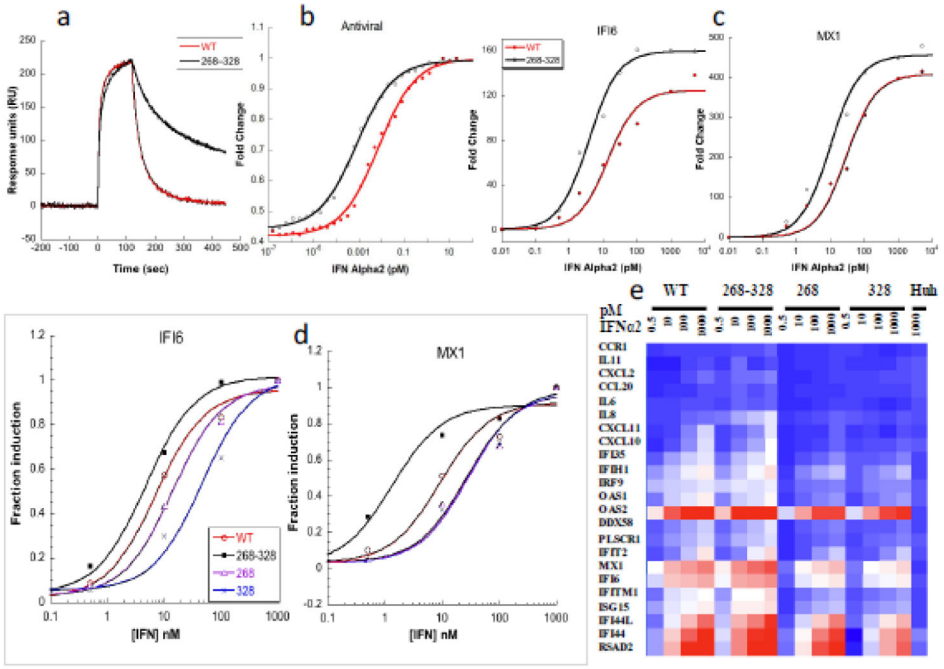

Fig. 6. Activity of the 268C-328C disulfide mutant of IFNAR1

(a) shows binding of the IFNa2 mutant YNS to purified WT and mutant IFNAR1 as determined by SPR (see also Fig. S2). **(b)** Antiviral activity after addition of the indicated amounts of IFN for 4 h before ECMV was added for 14 h. Cell survival was determined by crystal violet. **(c)** Gene expressions of stably transfected Huh7 cells after 16 hours treatment with indicated amounts of IFNα2. qPCR was then performed for IFI6 and MX1 genes. The data presented are the relative expression levels compared to those of untreated cells, normalized against HPRT1. **(d)** Gene induction, similar to panel C but with single cysteine receptors receptor mutations monitored. **(e)** Fold change in gene expression using the Fluidigm system (see Methods). Cells were treated as in C and cDNAs (50ng/ml) were preamplified with all the primers polled and analyzed with the BioMark real-time PCR instrument. The presented data are averages from 5 **(b)**, 6 **(c)**, 3 **(d)**, 2 **(e)** independent experiments.

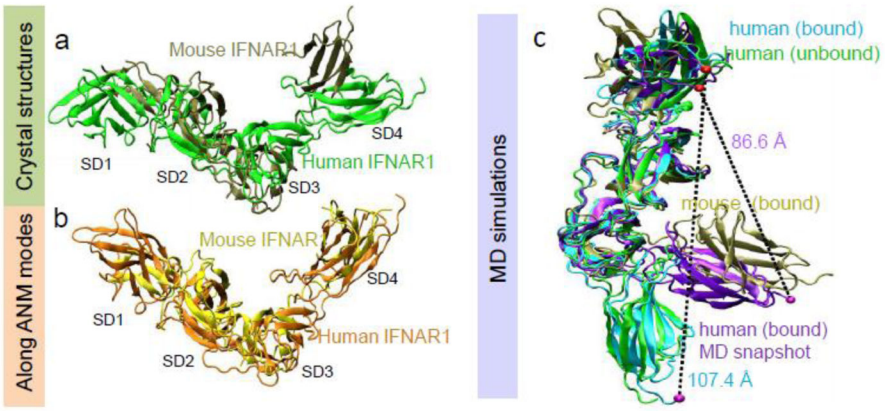

Fig. 7. Intrinsic ability of IFNAR1 structure to adapt to functional interactions

(a) IFNAR1 crystal structures resolved for mouse and human are easily exchangeable conformers favored by their common architecture. Superposition of human (unbound, *green*) and mouse (bound, *tan*; (PDB id: **3WCY**) structures yields an RMSD of 10.2 Å **(b)** Movements along the global modes reduce the RMSD to 6.5 Å. The diagrams represent the human (*orange*) and mouse (*yellow*) structures deformed along their ANM modes 1 and 3, respectively. **(c)** MD simulations of IFNAR1 confirm the adaptability of the receptor to sample the conformational space between the human and mouse structures. The figure displays a snapshot (*violet*) from MD simulations. The simulations were initiated from human IFNAR1 crystal structure in the bound state (*cyan*). SD4 undergoes a large displacement to reorient similarly to its conformation in the mouse structure. The distance between N23 (*red sphere*) and T407 (*magenta sphere*) decreases by approximately 20 Å during this reorientation.

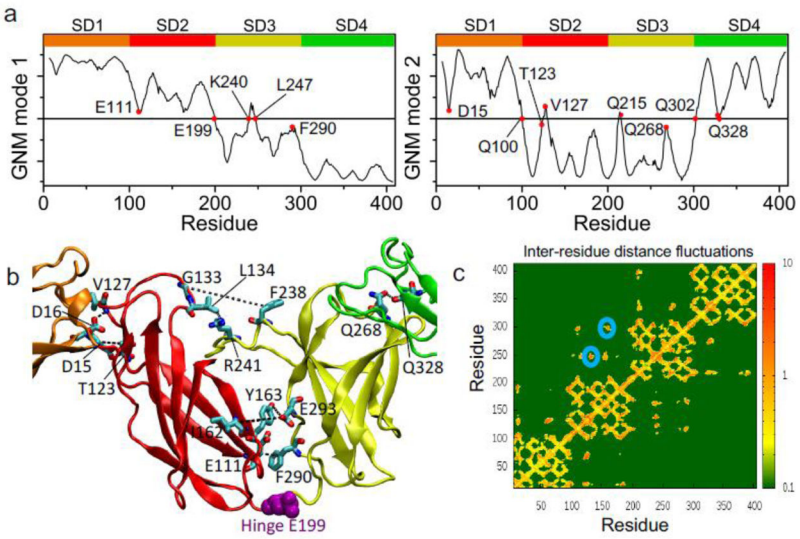

Fig. 8. GNM-based identification of key sites (global hinges) and key interactions in IFNAR1 EC domain

(a) Distribution of residue movements along global modes 1 (*left*) and 2 (*right*), predicted by the GNM. Hinge residues are located at the crossover ($y = 0$) between positive- and negative-direction motions: E199 (mode 1) and Q100 and Q302 (mode 2). Other key residues near the hinge centers (at $y \approx 0$) include E111 and K240-L247 (mode 1) and D15, T127, Q215, Q268 and Q328 (mode 2). **(b)** Location of key residues and interactions on the structure. The effect of locking these inter-subdomain interactions (by engineered disulfide bridges) on IFNAR1 binding and signaling properties is examined experimentally (see Table 1). Fig. S3 and Animations 5 and 6 show the inter-residue distance changes at three pairs of residues with large distances in structure. See also the zoom-in view for double mutants I162-E293 and Y163-E293 in Fig. S4. **(c)** Inter-residue distance fluctuations, shown for residue pairs separated by <15 Å in the folded structure. *Blue circles* highlight sequentially distant pairs (G133-F238 (and L134-R241) and I162-E293) distinguished by large distance fluctuations due to the SD2-SD3 global hinge motions.

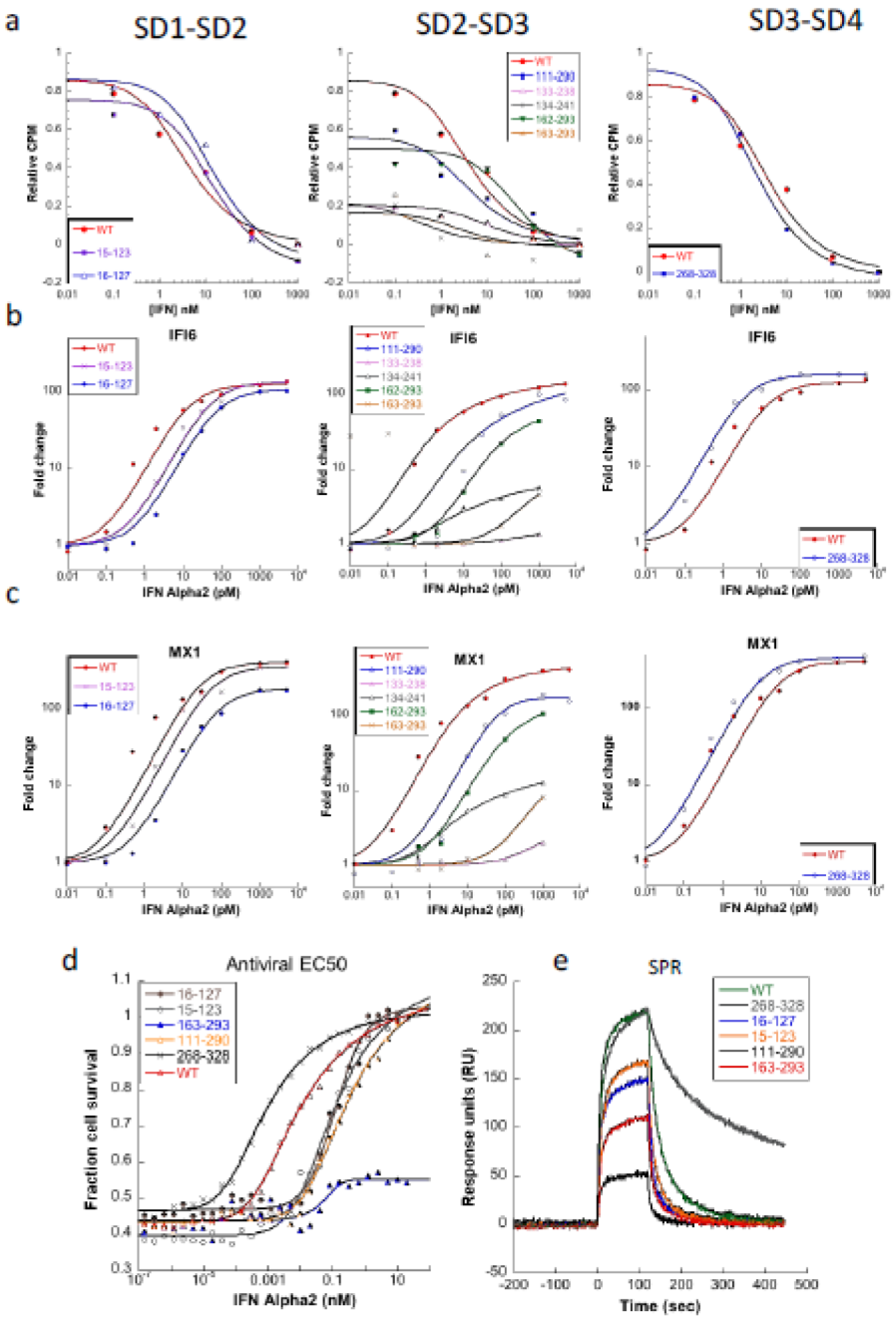

Fig. 9. Activity of 8 disulfide mutants of IFNAR1 located between domains SD1-SD2, SD2-SD3 and SD3-SD4

(a) Signal emitted from 1.5 nm I^{125}-labeled WT IFNα2 after competing with cold IFN at different concentrations. Y-axis represents the fraction of gamma signal relative to the signal in the absence of cold competitor. **(b)** and **(c)** IFI6 and MX1 gene expressions respectively of transfected Huh7 cells after 16 hours treatment with indicated amounts of IFNα2. The data presented are the relative expression levels compared to those of untreated cells, normalized against HPRT1. **(d)** Antiviral activity of stably transfected Huh7 cells after addition of the indicated amounts of IFN for 4 h before ECMV was added for 14 h. Cell

survival was determined by crystal violet. **(e)** Binding of 100 nM of the IFNa2 mutant YNS to purified WT and mutant IFNAR1 receptors as monitored by SPR. The presented data are averages from 3 **(a)**, 4 **(b – d)**, 2 **(e)** independent experiments.

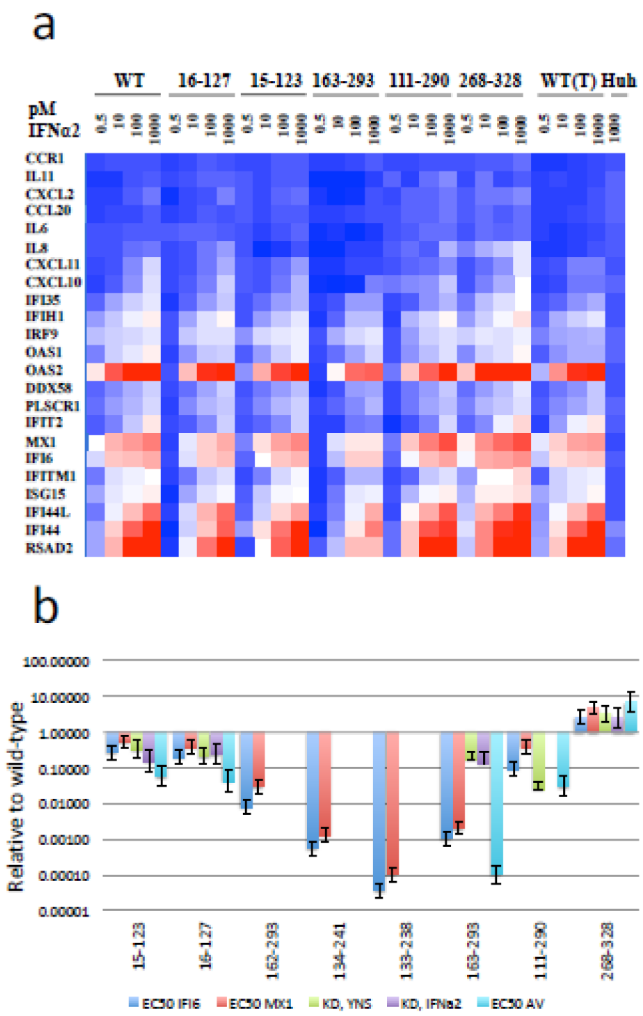

Fig. 10. Activity of the disulfide mutants of IFNAR1

(a) Fold change in gene expression using the fluidigm system (see methods). Transfected Huh7 Cells were treated for 16 h with indicated amounts of IFNα2 and cDNAs (50ng/ml) were preamplified with all the primers polled and analyzed with the BioMark real-time PCR instrument relative to HPRT1. Color code is blue to red, from no induction to maximal induction. **(b)** Summary of experimentally determined fold-change (relative to WT) of the data shown in Fig. 6 and Fig. 9 for the different examined activities of IFNAR1 disulfide bond mutations. K_D values were determined by SPR from 6 different analyte concentrations (e.g. see Fig. S2). The error bars represent 2x standard deviation of the relative mutant to wild-type data. Absolute values are provided in Table S1.

Table 1

Residue pairs located on opposite sides of GNM hinges selected for cross-linking experiments and functional assays

Subdomains	Res 1	Res 2	Dist[a] (Å)	ANM results					
				Mode	MaxVar (Å)[b]	Max d (Å)	Min d (Å)	E-Min d[c] (Å)	E2-Min d[d] (Å)
Set I – residue pairs predicted by ANM soft modes to alter global dynamics if cross-linked									
SD2-SD3	G133	F238	14.1	4	5.1	17.0	11.9	11.6	9.1
	L134	R241	8.2	4	2.1	9.4	7.3	7.4	6.7
	I162	E293	9.4	1	2.7	10.8	8.1	8.3	8.1
Set II – pairs located in the vicinity of hinge centers									
SD2-SD3	Y163	E293	7.6	2	0.7	8.2	7.5	6.0	6.2
	E111	F290	7.5	1	1.3	8.2	6.9	5.8	5.6
SD1-SD2	D15	T123	6.5	2	0.3	6.7	6.4	5.9	6.0
	D16	V127	6.4	4	0.2	6.6	6.4	6.5	6.6
SD3-SD4	Q268	Q328	6.8	4	0.4	7.1	6.7	8.2	8.3

[a] Distances between the two residues (based on C^{α} atoms) in the human IFNAR1 crystal structure, unbound form (PDB id: **3S98**) with modeled SD4

[b] MaxVar is the difference between the maximal and minimal distances (Max d and Min d) between the two residues in the examined mode (based on C^{a} atoms) using the scaling parameter a = 27;

[c] E-Min d is the value for Min d after energy minimization;

[d] E2-Min d is the closest separation attained after a 2^{nd} round of displacement along the same modes and energy minimization.